Prepared for submission to JCAP

The first AKRA mass map reconstruction from HSC Y1 data

Yuan Shi[a,c] **Pengjie Zhang**[a,b,c] **Zhao Chen**[a,c] **Jian Qin**[a,c] **Li Cui**[a,c] **Furen Deng**[d,e] **Ji Yao**[g]

[a]Department of Astronomy, School of Physics and Astronomy, Shanghai Jiao Tong University, Shanghai, 200240, China

[b]Division of Astronomy and Astrophysics, Tsung-Dao Lee Institute, Shanghai Jiao Tong University, Shanghai, 200240, China

[c]Key Laboratory for Particle Astrophysics and Cosmology (MOE) / Shanghai Key Laboratory for Particle Physics and Cosmology, China

[d]National Astronomical Observatories, Chinese Academy of Sciences, 20A Datun Road, Beijing 100101, P. R. China

[e]University of Chinese Academy of Sciences, School of Astronomy and Space Science, Beijing 100049, P. R. China

[g]Shanghai Astronomical Observatory (SHAO), Nandan Road 80, Shanghai, China

E-mail: yshi@sjtu.edu.cn, zhangpj@sjtu.edu.cn

Abstract. Weak lensing mass-mapping from shear catalogs faces systematic challenges from survey masks and spatially varying noise. To overcome these issues and reconstruct unbiased convergence κ maps, we have constructed the AKRA (Accurate Kappa Reconstruction Algorithm), a prior-free and maximum-likelihood based analytical method. It has been validated for mock shear catalogs with a variety of survey masks. In this work, we present the first real-data application of the AKRA on the Subaru Hyper Suprime-Cam Year 1 (HSC Y1) data. We first validate AKRA using mock shear catalogs from the `Kun` simulation suite, with masks corresponding to the six HSC Y1 regions (`GAMA09H`, `GAMA15H`, `HECTOMAP`, `VVDS`, `WIDE12H`, and `XMMLSS`). The investigated statistics, including the lensing power spectrum, $\langle\kappa^2\rangle$, $\langle\kappa^3\rangle$, and the one-point probability distribution function of κ, are all unbiased. We then apply AKRA to the HSC Y1 shear catalog and provide reconstructed κ maps ready for subsequent scientific analyses.

Contents

1 Introduction

Weak gravitational lensing (WL) directly measures the projected mass distribution in the Universe, and is therefore a powerful probe of structure growth and cosmology [1–6]. Over the past decade, stage-III weak-lensing surveys such as the Dark Energy Survey (DES; [7–9]), the Hyper Suprime-Cam Subaru Strategic Program (HSC; [10–12]), and the Kilo-Degree Survey (KiDS; [13, 14]) have achieved S/N$\sim$ 30 in cosmic shear measurements. The ongoing and upcoming stage-IV surveys will advance weak lensing into a new era, improving S/N by an order of magnitude or more (e.g, [15]). These include Euclid [16, 17], the Vera C. Rubin Observatory Legacy Survey of Space and Time (LSST; [18, 19]), the Roman Space Telescope [20], and the Chinese Space Station Telescope (CSST; [15, 21, 22]).

So far, most weak-lensing analyses in galaxy surveys have been performed directly using shear catalogs. However, for a variety of applications it is more convenient to work with convergence (κ) maps. First, many non-Gaussian statistics are naturally defined on κ fields. These include one-point probability distribution functions (PDFs), peak and void counts [23–25], skewness and kurtosis [26–28], Minkowski functionals [29–31] and scattering transform [32, 33]. Furthermore, both the conventional three-point correlation function and bispectrum [4, 34] and the recent techniques such as machine-learning [35–38], and field-level inference [39, 40] are more convenient to implement using the κ maps instead of shear catalogs. Second, in galaxy–galaxy lensing, the tangential shear $\gamma_t(\theta)$ is inherently nonlinear, as it includes contributions from scales $\theta' < \theta$. This intrinsic nonlinearity complicates the theoretical modeling [41–44]. In contrast, the κ-galaxy cross-correlation is free of this issue.

To convert a shear catalog into a convergence map, the Kaiser-Squires (KS) method [26, 45–47] is widely used. However, it suffers from biases in the presence of survey masks and spatially varying noise. Various alternative approaches to the KS method have been developed, including Bayesian forward modeling [48–50], Wiener filtering [51], sparsity- and lognormal-inspired methods [51–55], and wavelet reconstructions [56, 57]. These methods typically impose explicit assumptions about the statistical properties of the convergence field. Alternatively, we build the Accurate Kappa Reconstruction Algorithm (AKRA, [58, 59]). It is a prior-free and maximum-likelihood based analytical method, applicable to both flat and curved sky. Tests against various mock shear catalogs show that it delivers stable and unbiased κ reconstructions .

In this work, we present the fist application of AKRA to real data, using the first-year shear catalog from the Hyper Suprime-Cam Subaru Strategic Program (HSC Y1; [60]), which covers 136.9 deg^2 over six disjoint fields. This catalog has been widely used in recent studies of non-Gaussian weak-lensing statistics, including peak counts, Minkowski functionals, PDFs, and scattering transforms [61–68]. All of these studies have so far relied on the KS reconstructed convergence maps. Therefore κ maps reconstructed using methods other than KS would serve as independent checks for the above statistical analysis. AKRA passes all investigated tests against mock shear catalogs with HSC Y1 survey boundary, masks and spatially varying noise. Therefore we believe that the AKRA reconstructed mass maps are ready for subsequent scientific analysis. All maps in this work will be made publicly available upon the publication of this paper.

The paper is organized as follows. In Section 2, we present the formulation of AKRA and describe the mass map reconstruction pipeline. Section 3 introduces the HSC Y1 data set and presents the reconstructed convergence maps. In Section 4, we describe the simulation framework and validation tests. Section 5 provides our discussions and conclusions.

2 Method

In this work, we structure the analysis into two parts: (i) an observational part that reconstructs κ from the HSC Y1 shear catalog(Sec. 2); and (ii) a simulation part that creates HSC-like mocks to validate the reconstruction and quantify uncertainties (Sec. 4). Figure 1 summarizes the workflow.

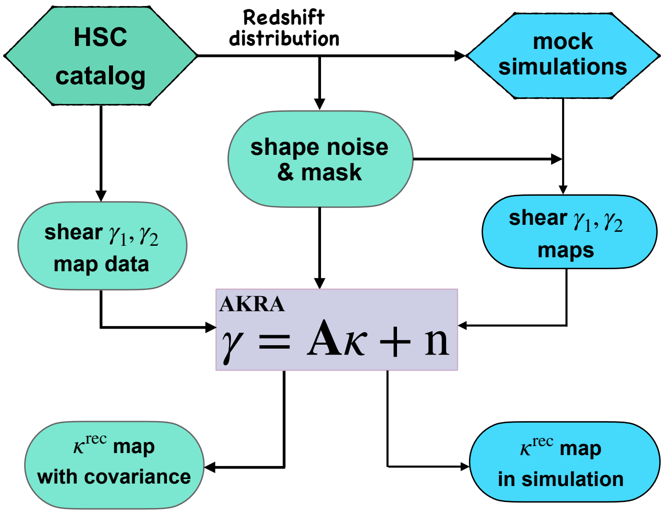

Figure 1. Overview of the mass map reconstruction pipeline. The left side shows the processing of HSC Y1 galaxy catalogs into shear maps and masked fields, while the right side shows parallel validation using mock simulations. The central AKRA module performs prior-free reconstruction of the convergence field.

The shear-convergence relation in the presence of masks and noise can be written as a linear system:

$$\boldsymbol{\gamma} = \mathbf{A}\,\boldsymbol{\kappa} + \boldsymbol{n}\,. \tag{2.1}$$

For HSC we can adopt the flat sky approximation and use the flat sky version of AKRA [58]. Then $\gamma = \begin{bmatrix} \tilde{\gamma}_1^m(\vec{L}) \\ \tilde{\gamma}_2^m(\vec{L}) \end{bmatrix}$ is the observed (masked) shear, $\boldsymbol{\kappa}$ is the true convergence, and $\boldsymbol{n}$ is noise. The linear operator $\mathbf{A}$ The operator $\mathbf{A}$ combines (i) the geometric lensing kernels, which project κ into (γ_1, γ_2) with angular factors $\cos 2\phi_\ell$ and $\sin 2\phi_\ell$ for each Fourier mode $\boldsymbol{\ell}$, and (ii) the mask-induced mode coupling through a Fourier-space mask operator $\mathbf{M}$.[1]

$$\mathbf{A} = \begin{bmatrix} \cos\left(2\phi_{\ell_1}\right) \mathbf{M} \\ \sin\left(2\phi_{\ell_1}\right) \mathbf{M}\, . \end{bmatrix}$$

The associated covariance of the estimator is then:

$$\mathbf{C} = \left(\mathbf{A}^{\mathrm{T}}\mathbf{N}^{-1}\mathbf{A}\right)^{-1}, \tag{2.2}$$

where $\mathbf{N} \equiv \langle \mathbf{n}\,\mathbf{n}^{\mathbf{T}} \rangle$ is the noise covariance matrix. $\mathbf{C}$ is often ill-conditioned, especially in the presence of large mask regions or incomplete sampling of Fourier modes. To regularize the inversion and suppress noise amplification, we adopt a small regularization matrix $\mathbf{R} = \lambda \mathbf{I}$ where $\lambda \sim 10^{-3}$. The estimator then becomes:

$$\hat{\boldsymbol{\kappa}} = \left(\mathbf{A}^{\mathrm{T}}\mathbf{N}^{-1}\mathbf{A} + \mathbf{R}\right)^{-1} \mathbf{A}^{\mathrm{T}}\mathbf{N}^{-1}\gamma. \tag{2.3}$$

In our previous work [58, 59], a simplified model with $\mathbf{N}^{-1} = \mathbf{I}$ was assumed, effectively treating the noise as homogeneous and uncorrelated. In this study, we go beyond this approximation by explicitly constructing $\mathbf{N}$ based on the spatially varying shear noise across the field, derived from the weighted shape noise in each pixel.

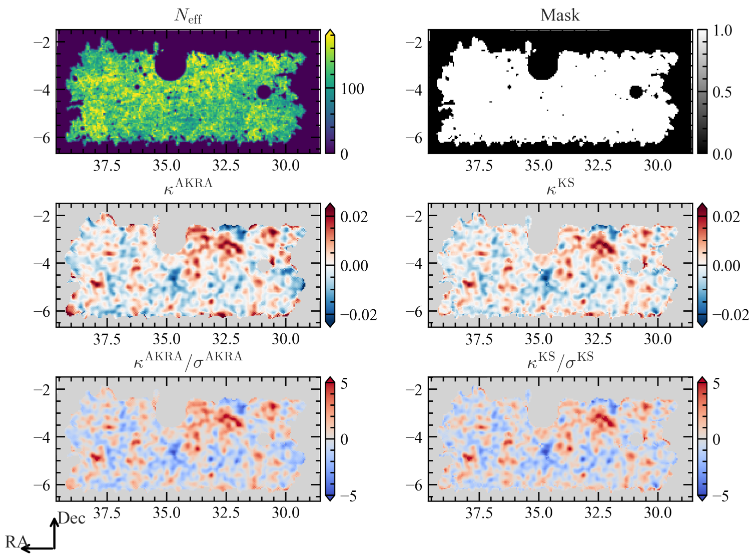

Figure 2. Weak lensing mass mapping results for the XMMLSS field with source galaxies in $z_{\mathrm{best}} \in (0.3, 1.5]$. Panels show (from left to right, top to bottom): (1) the effective source number density n_{eff}; (2) the binary mask derived from n_{eff} (pixels with $n_{\mathrm{eff}} < 10$ galaxies are excluded); (3) the AKRA reconstructed convergence κ^{AKRA}; (4) the KS convergence κ^{KS}; (5) the SNR map of κ^{AKRA}; (6) the SNR map of κ^{KS}. The convergence, and SNR maps are smoothed with a Gaussian window of $\sigma = 5$ arcmin for better demonstration.

[1] In the idealized case without masks (and noise-free), $\mathbf{M} \to \mathbf{I}$, AKRA reduces to KS [58, 59].

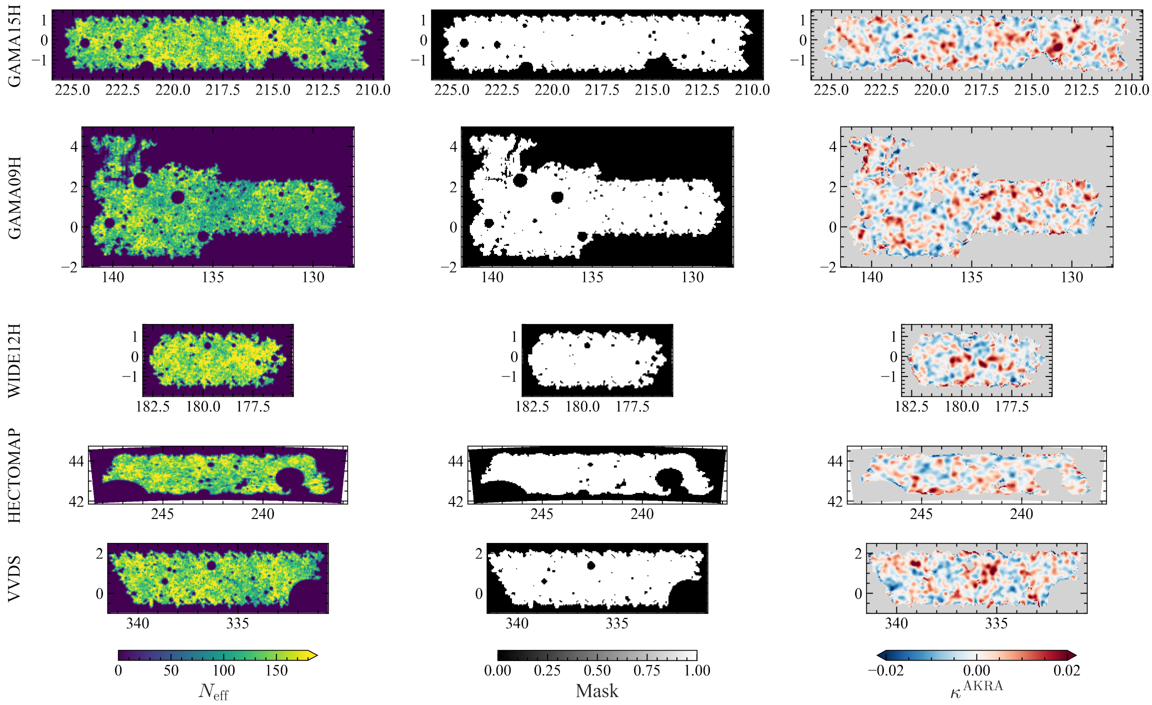

Figure 3. Overview of mass mapping results in the five representative HSC-Y1 fields: `GAMA15H`, `GAMA09H`, `WIDE12H`, `HECTOMAP`, and `VVDS`. For each field, panels (from left to right) show the effective source density $n_{\rm eff}$, the binary mask, and the AKRA reconstructed convergence maps $\kappa^{\rm AKRA}$. The convergence maps are smoothed with a Gaussian window of $\sigma = 5$ arcmin for demonstration.

3 HSC Y1 Data Results

The first-year data release of the HSC Y1 shear catalog [60] covers an area of 136.9 deg^2 across six disjoint Wide fields: `GAMA09H`, `GAMA15H`, `HECTOMAP`, `VVDS`, `WIDE12H`, and `XMMLSS`. It contains shape measurements and shear estimates for approximately 12.1 million galaxies. We adopt Photometric redshifts (photo-z) from the best estimate of `Ephor AB` algorithm [69], denoted as $z_{\rm best}$. Sources are restricted to the range $0.3 < z_{\rm best} \leq 1.5$. [2] The effective number of source galaxies in a given pixel is defined as

$$N_{\rm eff} = \sum_{i \in {\rm pix}} \frac{\sigma^2_{{\rm SN},i}}{\sigma^2_{{\rm SN},i} + \sigma^2_{m,i}} ,$$

where $\sigma_{{\rm SN},i}$ and $\sigma_{m,i}$ denote the intrinsic shape noise and measurement error of galaxy i, respectively. The average effective source density $n_{\rm eff} = N_{\rm eff}/\Omega \simeq 17$ arcmin^{-2}. The corresponding shear noise variance is given by $\sigma^2_{\rm pix} = \sigma^2_\gamma / N_{\rm eff}$, with $\sigma_\gamma \simeq 0.24$ being the intrinsic shape noise of HSC Y1 source galaxies.

For the reconstruction, we adopt a flat-sky grid with 3 arcmin pixels. Fig. 2 shows the $N_{\rm eff}$ map of the `XMMLSS` region, which is highly inhomogeneous. Together with the complicated survey boundary, they represent a major issue to be dealt with. We also need to define the binary mask $m(\vec{\theta})$. $m = 1$ if $N_{\rm eff} > N_{\rm thres}$ and 0 otherwise. For a pixel size of $3' \times 3'$, the average $N_{\rm eff}$ is 153. We

[2]The public HSC Y1 catalog also provides six alternative photo-z estimates per galaxy: `MLZ, Ephor, Mizuki, NNPZ, Frankenz, DEmP`. We choose `Ephor AB` following the HSC Y1 cosmology analyses [70, 71].

adopt $N_{\rm thres} = 10$ to disregard pixels of large noise. This cut only disregards $\sim 0.1\%$ of galaxies[3], but ensures numerical stability in the reconstruction. Fig. 2 shows the mask map in the XMMLSS region. For the reconstruction we adopt a small diagonal regularization term $\mathbf{R} = \lambda \mathbf{I}$ with $\lambda = 10^{-3}$. Noise properties are characterized using 300 randomized shear realizations obtained by randomizing galaxy orientations while keeping their positions and weights fixed. The pixel-level noise of the reconstructed convergence field, σ_κ, is then estimated from the variance of reconstructed κ across these realizations.

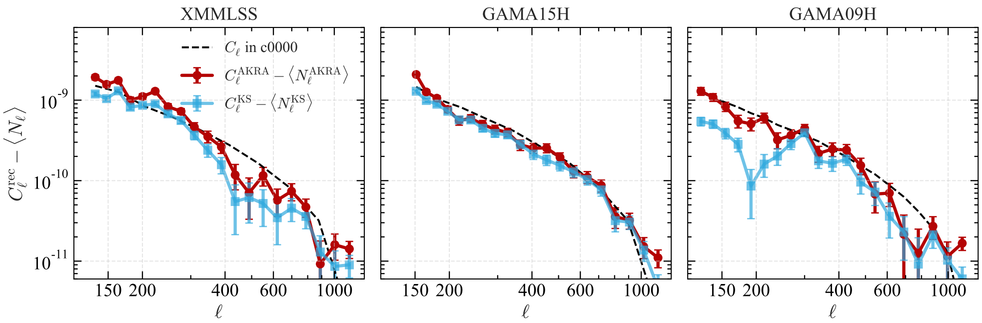

Figure 4. Power spectrum of the reconstructed convergence maps from HSC Y1 data in the redshift range $0.3 < z_s \leq 1.5$. From left to right, we show results for three large fields: XMMLSS, GAMA15H and GAMA09H. The error bars are estimated from 300 noise realizations per field. The black dashed curves indicate the theoretical power spectrum for a fiducial ΛCDM cosmology, shown for reference rather than as a best-fit model.

3.1 Mass mapping results

We then apply AKRA to all six HSC Y1 fields, yielding the first set of convergence (κ) maps from this method on real survey data. Figs. 2 and 3 illustrate the complex survey masks and strong spatial variations in source density across the HSC Y1 fields, together with the reconstructed κ maps.

As a representative example, we highlight the XMMLSS region in Fig. 2. For comparison, we also perform KS reconstructions on the same grids. In well-sampled interior regions, AKRA and KS recover consistent large-scale structures, and the overall pattern of peaks and voids agrees. Near survey boundary and around masks, the reconstructions differ more significantly. Since the shear-convergence relation is non-local in real space, masks in the shear catalog impact the reconstruction of convergence in the unmasked regions in KS method. In contrast, AKRA incorporates the survey mask directly into a prior-free maximum-likelihood framework, yielding minimum-variance estimates of the convergence field under realistic survey conditions. The accuracy of AKRA in handling mask effects has been validated with dedicated simulations in previous work [58].

The corresponding power spectra are presented in Fig. 4; error bars are estimated from 300 noise realizations per field. These κ maps and their power spectra constitute the primary data products released in this work and provide the basis for subsequent scientific analyses. Here we focus on presenting the reconstructed maps and derived data products from real HSC Y1 observations. A full cosmological interpretation from these results will require rigorous treatment of observational systematics, including photo-z uncertainties, shear calibration, and intrinsic alignments, to be addressed in future work.

[3]For reference, more aggressive thresholds would discard substantially more information (1.4% for $N_{\rm thres} = 50$, 6.3% for $N_{\rm thres} = 100$, and $\sim$50% for $N_{\rm thres} = 150$).

4 Validation with Simulations

To quantify the accuracy of AKRA reconstruction of HSC Y1, we perform validation tests using mock simulations with known input convergence fields. They allow us to evaluate both the statistical accuracy of the reconstructed maps and examine whether AKRA faithfully reproduces the non-Gaussian characteristics of the underlying matter field.

The mock convergence fields are generated from the high-resolution KUN simulation suite [72], which is part of the JIUTIAN program designed in preparation for the forthcoming CSST cosmological survey [73]. The KUN suite consists of 129 N-body simulations spanning an eight-dimensional cosmological parameter space, including models with dynamic dark energy and massive neutrinos. It has been widely used to build cosmological emulators for the matter power spectrum, halo mass function, and biased tracer spectra [72, 74, 75]. In this work, we adopt the fiducial realization (c0000) from the suite, with cosmological parameters $\Omega_M = \Omega_{\rm cb} + \Omega_\nu = 0.3111$, $\Omega_b = 0.0490$, $H_0 = 67.66$ km s^{-1} Mpc^{-1}, $n_s = 0.9665$, $\sigma_8 = 0.81$, and a dark energy equation of state of $w = -1$, $w_a = 0$, with a total neutrino mass of $\Sigma m_\nu = 0.06$ eV. Convergence maps are generated by stacking the full-sky projected density maps with thickness $50\,h^{-1}$Mpc in the on-the-fly lightcone. The corresponding shear components (γ_1, γ_2) are then obtained. The mock simulations also adopt the same photo-z distribution as the HSC Y1 data. We emphasize that throughout this section we adopt only the fiducial cosmology of the KUN suite, without exploring the full parameter space.

For each of the six HSC Y1 fields, we generate 200 realizations that reproduce the survey geometry, pixelization, binary mask, and spatially varying effective number map $N_{\rm eff}(\vec{\theta})$ measured from the data (Section 3). Each realization includes the input cosmological shear signal (γ_1, γ_2), to which we apply the survey mask and add pixel-dependent shape noise. We reconstruct the convergence maps using both the AKRA and KS methods with the same settings as applied to the data. Noise-only maps (without cosmological signal) are also generated in the same way to estimate noise biases.

4.1 Power spectrum results

The angular power spectrum provides a direct two-point diagnostic of reconstruction accuracy. For each mock, we measure (i) the auto-spectrum of the reconstructed convergence map and (ii) its cross-spectrum with the input ("true") convergence over the unmasked region. We quantify performance using the ratios

$$\frac{C_\ell^{\rm rec}}{C_\ell^{\rm true}}, \qquad \frac{C_\ell^{\rm rec\text{-}true}}{C_\ell^{\rm true}},$$

where $C_\ell^{\rm true}$ is the spectrum of the true field, $C_\ell^{\rm rec}$ is the noise-subtracted auto-spectrum of the reconstruction, and $C_\ell^{\rm rec\text{-}true}$ is the cross-spectrum. Amplitude biases in $C_\ell^{\rm rec}$ can, in principle, be corrected by rescaling individual ℓ-modes, whereas phase errors probed by $C_\ell^{\rm rec\text{-}true}$ cannot. This makes achieving an unbiased $C_\ell^{\rm rec\text{-}true}/C_\ell^{\rm true}$ the more challenging requirement.

As shown in Fig. 5, AKRA shows unbiased recovery over $200 \lesssim \ell \lesssim 1000$: both ratios are consistent with unity within 5% when averaged over realizations, demonstrating accurate reconstruction of both amplitude and phase information. In contrast, KS exhibits a systematic $\sim 20\%$ suppression of power across all scales, with the largest deficit on large scales where mask-induced mode mixing is strongest. In previous tests [58, 59], similar analyses were performed using idealized mocks that included survey masks but neglected shape noise. Here we extend the validation to realistic conditions by incorporating both irregular masks and spatially varying noise, which together constitute the dominant observational challenges for weak-lensing mass mapping.

Crucially, the unbiased recovery demonstrated here will become even more valuable in future wide-field surveys (e.g., LSST, Euclid, CSST). With higher source densities and larger sky coverage,

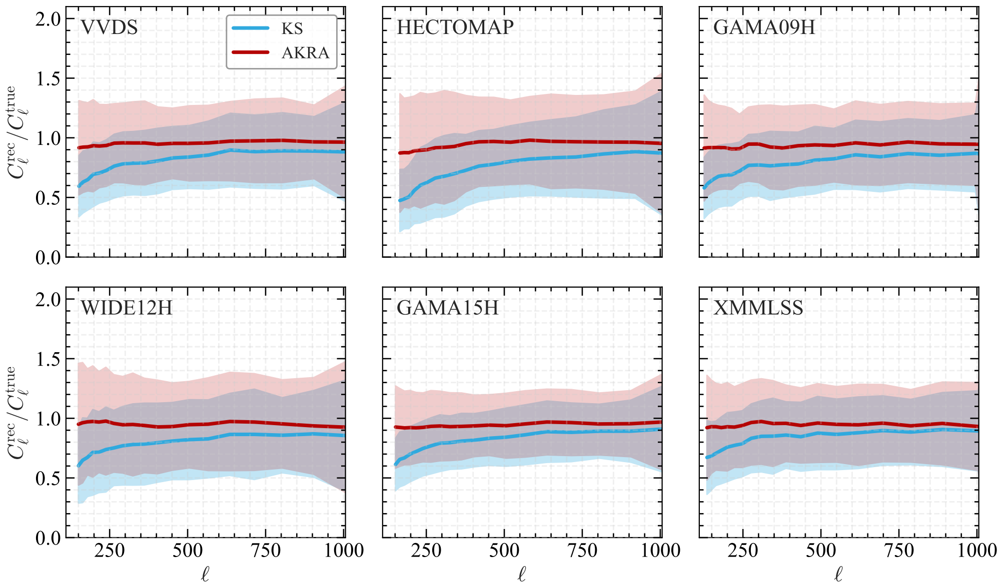

(a)

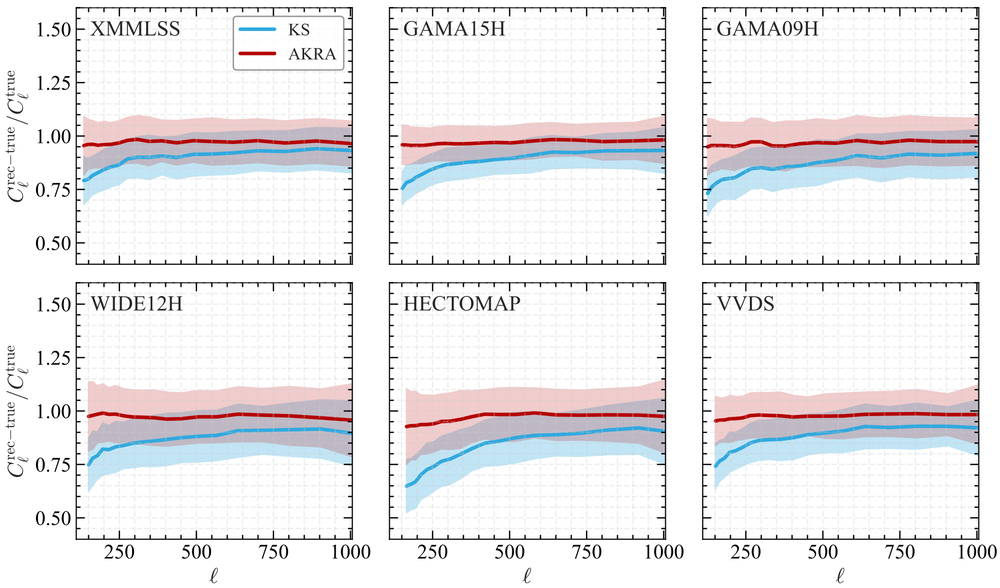

(b)

Figure 5. Validation of reconstructed convergence power spectra from mock simulations. Panel (a) shows the ratio of noise-subtracted auto-spectra $C_\ell^{\rm rec}/C_\ell^{\rm true}$, and panel (b) shows the ratio of cross-spectra $C_\ell^{\rm rec\text{–}true}/C_\ell^{\rm true}$ between reconstructed and true fields. Results are averaged over 200 realizations per field, with error bars indicating the standard deviation. AKRA (in red) follows the true input spectrum across a broad multipole range, demonstrating that its treatment of masks and spatially varying noise preserves both large- and small-scale modes. KS (in blue), in contrast, underestimates power on all scales, especially on large scales. This difference illustrates that explicitly modeling the mask, as done in AKRA, is essential for an unbiased recovery of the convergence field.

these surveys will achieve higher S/N and make AKRA a promising tool for producing reliable convergence maps.

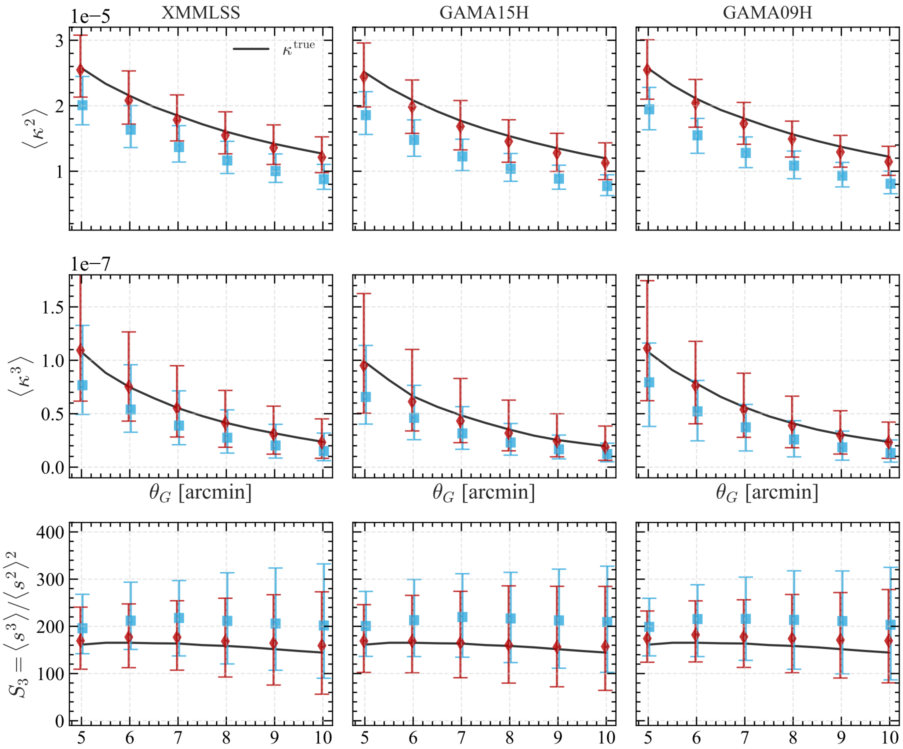

Figure 6. Higher-order statistics of reconstructed convergence fields from mock simulations in three representative HSC Y1 regions (`XMMLSS`, `GAMA15H`, `GAMA09H`). From top to bottom: the second moment $\langle\kappa^2\rangle$, the third moment $\langle\kappa^3\rangle$, and the normalized skewness $S_3 = \langle\kappa^3\rangle/\langle\kappa^2\rangle^2$. The x-axis shows the Gaussian smoothing scale $\theta_G \in \{5, 6, 7, 8, 9, 10\}$ arcmin. Black curves are measured from the true input maps; blue squares and red diamonds correspond to KS and AKRA reconstructions, respectively. Error bars indicate the scatter across 200 mock realizations per field. AKRA closely reproduces the true higher-order moments for every θ_G considered, in contrast to KS, which systematically biased the signal at all scales. These tests demonstrate that AKRA preserves non-Gaussian features of the convergence field, enabling analyses beyond two-point statistics.

4.2 Skewness and PDF results

The mass maps become increasingly non-Gaussian on small scales due to non-linear structure growth. Higher-order statistics are therefore needed to capture this information. In this work, we use the skewness and one-point probability distribution function (PDF) as field-level diagnostics of whether AKRA preserves the non-linear features of the convergence field.

4.2.1 Skewness

Skewness, defined as the normalized third moment [76],

$$S_3 = \frac{\langle\kappa^3\rangle}{\langle\kappa^2\rangle^2}, \tag{4.1}$$

and quantifies the asymmetry of the convergence distribution. In perturbation theory, S_3 arises from non-linear mode coupling driven by gravitational instability and depends only weakly on the overall

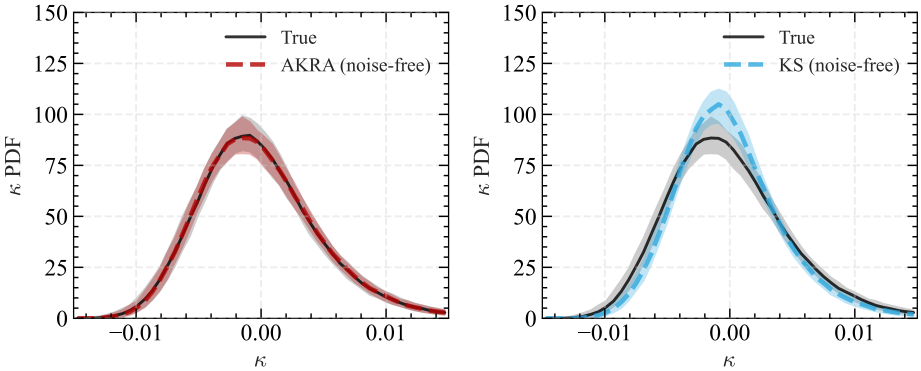

Figure 7. PDFs of reconstructed convergence fields from mock simulations in the representative HSC Y1 region `XMMLSS`. Here we show noise-free reconstructions with the real survey mask applied (same pixelization and mask as in the data.) As we can see from the figure, AKRA closely matches the true PDF and preserves the non-Gaussian features of the field. In contrast, the KS reconstruction is biased: the PDF is enhanced near $\kappa \approx 0$ and the tails are suppressed. Due to the limited S/N of HSC Y1, we do not show noisy PDFs here; a fair comparison would require additional noise deconvolution.

fluctuation amplitude, while receiving significant contributions from the high-κ tail associated with rare massive halos.

We compute the second and third moments from AKRA reconstructions in three representative HSC Y1 regions, estimating and subtracting the noise bias using 200 noise-only realizations. Figure 6 shows that AKRA accurately recovers the full dynamic range of both $\langle\kappa^2\rangle$ and $\langle\kappa^3\rangle$ across all smoothing scales considered, and hence yields unbiased estimates of S_3. In contrast, KS systematically underestimates both moments and consequently overestimates $S_3 = \langle\kappa^3\rangle/\langle\kappa^2\rangle^2$, typically requiring additional calibration to correct its amplitude bias. The excellent agreement between AKRA and the truth demonstrates that AKRA preserves the non-Gaussian information encoded in skewness.

4.2.2 PDFs

The one-point convergence PDF, $P(\kappa)$, provides a complementary characterization of non-Gaussianity. Its high-κ tail is dominated by the one-halo contribution from massive halos, while its negative tail arises from large-scale underdensities and voids. This makes $P(\kappa)$ sensitive to both the amplitude of matter fluctuations and the growth of non-linear structure. Theoretical descriptions include large-deviation theory [77–79] and phenomenological lognormal models [80].

We measure the PDF from reconstructed κ maps in noise-free mocks to isolate reconstruction effects. Figure 7 shows the convergence PDFs in the representative `XMMLSS` field. We compare the PDFs of the true, AKRA-reconstructed, and KS-reconstructed κ maps under noise-free conditions, applying the real survey mask. The KS reconstruction shows a clear bias: the PDF is enhanced near $\kappa \approx 0$, while both the positive and negative tails are suppressed. In contrast, AKRA closely reproduces the shape of the true PDF, including the extended positive and negative tails characteristic of the non-Gaussian convergence field, as shown in Fig. 7.

In real data, intrinsic galaxy ellipticities introduce shape noise that propagates into the convergence field. Including intrinsic shape noise would broaden the PDF and suppress its non-Gaussian features, making it difficult to clearly evaluate the differences between the AKRA and KS reconstructions. For a fixed smoothing scale and weighting scheme, the noisy one-point PDF is well approximated as the convolution of the underlying (noise-free) PDF with a zero average but nonnegligible variance [e.g. 79, 81]. For HSC Y1, the noise level is high that the shape noise would dominate. We therefore restrict the PDF test to noise-free mocks; a full treatment including noise deconvolution will be presented in future work.

5 Discussion and conclusion

We report the first application of AKRA to HSC Y1, yielding weak-lensing convergence maps for all six survey regions. The reconstruction pipeline was validated using realistic mock shear catalogs that reproduce the survey boundaries, masks, and spatially varying noise properties of HSC Y1. AKRA performs the shear-to-convergence inversion directly, accurately recovering the mass maps, ensuring unbiased recovery of two-point and non-Gaussian statistics under realistic conditions. We publicly release a complete set of κ-map products for each region, including reconstructed convergence maps, survey masks, effective number-density maps ($n_{\rm eff}$), SNR maps, and power spectra. These products are ready for a range of scientific applications, such as cross-correlations with other tracers and non-Gaussian statistical analyses.

This work validates AKRA on real survey data and delivers accurate convergence maps for scientific analyses. The limited S/N of HSC Y1 also poses challenges in deriving competitive cosmological constraints. Tomography divides sources into redshift bins to reconstruct redshift-dependent κ maps, which improves constraints but reduces the effective number density per bin and increases shape noise. Robust cosmological analysis further requires a blinded, end-to-end likelihood that properly accounts for observational systematics (photometric redshifts, shear calibration, PSF leakage, baryonic effects, and intrinsic alignments). In future work, we will apply AKRA to HSC Y3 and DES to perform tomographic reconstructions and obtain cosmological constraints.

Our results show that higher-order statistics, such as skewness and the one-point PDF, are sensitive to the reconstruction method. AKRA preserves these non-Gaussian features under realistic conditions and provides a robust framework for field-level mass mapping. Non-Gaussian statistics derived from AKRA κ maps offer a promising way to extract cosmological information beyond two-point statistics and to explore the origin of the S_8 tension between weak lensing and CMB results. The reconstructed κ field itself becomes an essential dataset that enables non-Gaussian analyses, cross-correlations, and future cosmological inference. We anticipate AKRA to be broadly applicable to current and upcoming weak-lensing surveys, and to support the construction of a comprehensive convergence-map data library that will provide accurate κ maps for cosmological and cross-correlation studies.

Acknowledgments

This work was supported by the National Key R&D Program of China (2023YFA1607800, 2023YFA1607801, 2020YFC2201602, 2022YFF0503403), the China Manned Space Project (#CMS-CSST-2021-A02), China Manned Space Program (#CMS-CSST-2025-A03), and the Fundamental Research Funds for the Central Universities. YS acknowledges the support from NSFC Grant No. 12503004. JY acknowledges the support from NSFC grant No. 12203084 and No. 12573006. This work made use of the Gravity Supercomputer at the Department of Astronomy, Shanghai Jiao Tong University. The results in this paper have been derived using the following packages: Numpy [82], Scipy [83], `HEALPix` [84], IPython [85] and CCL [86].

References

[1] M. Bartelmann and P. Schneider, Weak gravitational lensing, Physics Report **340** (2001) 291.

[2] A. Refregier, Weak gravitational lensing by large-scale structure, in Annual Review of Astronomy and Astrophysics, vol. 41, pp. 645–668, 2003, DOI.

[3] D. Munshi, P. Valageas, L. van Waerbeke and A. Heavens, Cosmology with weak lensing surveys, Physics Reports **462** (2008) 67.

[4] L.P. Fu and Z.H. Fan, Probing the dark side of the universe with weak gravitational lensing effects, Research in Astronomy and Astrophysics **14** (2014) 1061.

[5] M. Kilbinger, Cosmology with cosmic shear observations: A review, Reports on Progress in Physics **78** (2015) .

[6] R. Mandelbaum, Weak lensing for precision cosmology, Annual Review of Astronomy and Astrophysics **56** (2018) 393.

[7] T. Abbott, F.B. Abdalla, J. Aleksić, S. Allam, A. Amara, D. Bacon et al., The dark energy survey: More than dark energy - an overview, Monthly Notices of the Royal Astronomical Society **460** (2016) 1270.

[8] A. Amon, D. Gruen, M.A. Troxel, N. Maccrann, S. Dodelson, A. Choi et al., Dark energy survey year 3 results: Cosmology from cosmic shear and robustness to data calibration, Physical Review D **105** (2022) .

[9] L.F. Secco, S. Samuroff, E. Krause, B. Jain, J. Blazek, M. Raveri et al., Dark energy survey year 3 results: Cosmology from cosmic shear and robustness to modeling uncertainty, Physical Review D **105** (2022) .

[10] H. Aihara, R. Armstrong, S. Bickerton, J. Bosch, J. Coupon, H. Furusawa et al., First data release of the hyper suprime-cam subaru strategic program, Publications of the Astronomical Society of Japan **70** (2018) .

[11] C. Hikage, M. Oguri, T. Hamana, S. More, R. Mandelbaum, M. Takada et al., Cosmology from cosmic shear power spectra with subaru hyper suprime-cam first-year data, Publications of the Astronomical Society of Japan **71** (2019) .

[12] T. Hamana, M. Shirasaki, S. Miyazaki, C. Hikage, M. Oguri, S. More et al., Cosmological constraints from cosmic shear two-point correlation functions with hsc survey first-year data, Publications of the Astronomical Society of Japan **72** (2020) .

[13] K. Kuijken, C. Heymans, H. Hildebrandt, R. Nakajima, T. Erben, J.T.A. De Jong et al., Gravitational lensing analysis of the kilo-degree survey, Monthly Notices of the Royal Astronomical Society **454** (2015) 3500.

[14] M. Asgari, C.A. Lin, B. Joachimi, B. Giblin, C. Heymans, H. Hildebrandt et al., Kids-1000 cosmology: Cosmic shear constraints and comparison between two point statistics, Astronomy and Astrophysics **645** (2021) .

[15] J. Yao, H. Shan, R. Li, Y. Xu, D. Fan, D. Liu et al., Csst wl preparation i: forecast the impact from non-gaussian covariances and requirements on systematics control, Monthly Notices of the Royal Astronomical Society **527** (2024) 5206.

[16] R. Laureijs, J. Amiaux, S. Arduini, J.L. AuguŠres, J. Brinchmann, R. Cole et al., Euclid definition study report, Arxiv (2011) .

[17] C. Euclid, Y. Mellier, Abdurro'uf, J.A.A. Barroso, A. Achucarro, J. Adamek et al., Euclid. i. overview of the euclid mission, .

[18] L.S. Collaboration, P.A. Abell, J. Allison, S.F. Anderson, J.R. Andrew, J.R.P. Angel et al., Lsst science book, version 2.0, December 01, 2009, 2009. 10.48550/arXiv.0912.0201.

[19] Ž. Ivezić, S.M. Kahn, J.A. Tyson, B. Abel, E. Acosta, R. Allsman et al., Lsst: From science drivers to reference design and anticipated data products, Astrophysical Journal **873** (2019) .

[20] D. Spergel, N. Gehrels, C. Baltay, D. Bennett, J. Breckinridge, M. Donahue et al., Wide-field infrared survey telescope-astrophysics focused telescope assets wfirst-afta 2015 report, March 01, 2015, 2015. 10.48550/arXiv.1503.03757.

[21] Y. Gong, X. Liu, Y. Cao, X. Chen, Z. Fan, R. Li et al., Cosmology from the chinese space station optical survey (css-os), ASTROPHYSICAL JOURNAL **883** (2019) .

[22] H. Zhan, The wide-field multiband imaging and slitless spectroscopy survey to be carried out by the survey space telescope of china manned space program, Kexue Tongbao/Chinese Science Bulletin **66** (2021) 1290.

[23] H. Shan, X. Liu, H. Hildebrandt, C. Pan, N. Martinet, Z. Fan et al., KiDS-450: cosmological constraints from weak lensing peak statistics - I. Inference from analytical prediction of high sign Monthly Notices of the Royal Astronomical Society **474** (2018) 1116 [1709.07651].

[24] N. Martinet, P. Schneider, H. Hildebrandt, H. Shan, M. Asgari, J.P. Dietrich et al., KiDS-450: cosmological constraints from weak-lensing peak statistics - II: Inference from shear peaks using N-body simu Monthly Notices of the Royal Astronomical Society **474** (2018) 712 [1709.07678].

[25] D.Z. Liu, X.M. Meng, X.Z. Er, Z.H. Fan, M. Kilbinger, G.L. Li et al., Potential scientific synergies in weak lensing studies between the CSST and Euclid space probes, Astronomy & Astrophysics **669** (2023) A128 [2210.16341].

[26] L. Van Waerbeke, J. Benjamin, T. Erben, C. Heymans, H. Hildebrandt, H. Hoekstra et al., CFHTLenS: mapping the large-scale structure with gravitational lensing, Monthly Notices of the Royal Astronomical Society **433** (2013) 3373 [1303.1806].

[27] A. Petri, J. Liu, Z. Haiman, M. May, L. Hui and J.M. Kratochvil, Emulating the CFHTLenS weak lensing data: Cosmological constraints from moments and Minkowski functionals, Physical Review D **91** (2015) 103511 [1503.06214].

[28] C. Chang, A. Pujol, B. Mawdsley, D. Bacon, J. Elvin-Poole, P. Melchior et al., Dark Energy Survey Year 1 results: curved-sky weak lensing mass map, Monthly Notices of the Royal Astronomical Society **475** (2018) 3165 [1708.01535].

[29] J.M. Kratochvil, E.A. Lim, S. Wang, Z. Haiman, M. May and K. Huffenberger, Probing cosmology with weak lensing Minkowski functionals, Physical Review D **85** (2012) 103513 [1109.6334].

[30] M. Vicinanza, V.F. Cardone, R. Maoli, R. Scaramella, X. Er and I. Tereno, Minkowski functionals of convergence maps and the lensing figure of merit, Physical Review D **99** (2019) 043534 [1905.00410].

[31] D. Zürcher, J. Fluri, R. Sgier, T. Kacprzak and A. Refregier, Cosmological forecast for non-gaussian statistics in large-scale weak lensing surveys, Journal of Cosmology and Astroparticle Physics **2021** (2021) 028–028.

[32] S. Cheng, Y.S. Ting, B. Menard and J. Bruna, A new approach to observational cosmology using the scattering transform, MONTHLY NOTICES OF THE ROYAL ASTRONOMICAL SOCIETY **499** (2020) 5902.

[33] S. Cheng and B. Ménard, Weak lensing scattering transform: dark energy and neutrino mass sensitivity, MONTHLY NOTICES OF THE ROYAL ASTRONOMICAL SOCIETY **507** (2021) 1012.

[34] M. Takada and B. Jain, Three-point correlations in weak lensing surveys: Model predictions and applications, MONTHLY NOTICES OF THE ROYAL ASTRONOMICAL SOCIETY **344** (2003) 857.

[35] A. Gupta, J.M.Z. Matilla, D. Hsu and Z. Haiman, Non-Gaussian information from weak lensing data via deep learning, Physical Review D **97** (2018) 103515 [1802.01212].

[36] D. Ribli, B.Á. Pataki and I. Csabai, An improved cosmological parameter inference scheme motivated by deep learning, Nature Astronomy **3** (2019) 93 [1806.05995].

[37] J. Fluri, T. Kacprzak, A. Lucchi, A. Schneider, A. Refregier and T. Hofmann, Full w CDM analysis of KiDS-1000 weak lensing maps using deep learning, Physical Review D **105** (2022) 083518 [2201.07771].

[38] T. Lu, Z. Haiman and X. Li, Cosmological constraints from HSC survey first-year data using deep learning, Monthly Notices of the Royal Astronomical Society **521** (2023) 2050 [2301.01354].

[39] A.J. Zhou, X. Li, S. Dodelson and R. Mandelbaum, Accurate field-level weak lensing inference for precision cosmology, Phys. Rev. D **110** (2024) 023539.

[40] J. Zeghal, D. Lanzieri, F. Lanusse, A. Boucaud, G. Louppe, E. Aubourg et al., Simulation-based inference benchmark for weak lensing cosmology, Astronomy and Astrophysics **699** (2025) A327.

[41] T. Baldauf, R.E. Smith, U. Seljak and R. Mandelbaum, Algorithm for the direct reconstruction of the dark matter correlation function from weak lensing and galaxy clustering, PHYSICAL REVIEW D **81** (2010) 063531 [0911.4973].

[42] N. MacCrann, J. Blazek, B. Jain and E. Krause, Controlling and leveraging small-scale information in tomographic galaxy-galaxy lensing, Mon. Not. Roy. Astron. Soc **491** (2020) 5498 [1903.07101].

[43] Y. Park, E. Rozo and E. Krause, Localizing Transformations of the Galaxy-Galaxy Lensing Observable, Physical Review Letters **126** (2021) 021301 [2004.07504].

[44] J. Prat, J. Blazek, C. Sánchez, I. Tutusaus, S. Pandey, J. Elvin-Poole et al., Dark energy survey year 3 results: High-precision measurement and modeling of galaxy-galaxy lensing, PHYSICAL REVIEW D **105** (2022) 083528 [2105.13541].

[45] N. Kaiser and G. Squires, Mapping the dark matter with weak gravitational lensing, Astrophysical Journal **404** (1993) 441.

[46] V. Vikram, C. Chang, B. Jain, D. Bacon, A. Amara, M.R. Becker et al., Wide-field lensing mass maps from dark energy survey science verification data: Methodology and detailed analysis, Physical Review D - Particles, Fields, Gravitation and Cosmology **92** (2015) .

[47] M. Gatti, B. Jain, C. Chang, M. Raveri, D. Zürcher, L. Secco et al., Dark energy survey year 3 results: Cosmology with moments of weak lensing mass maps, PHYSICAL REVIEW D **106** (2022) .

[48] J. Alsing, A. Heavens, A.H. Jaffe, A. Kiessling, B. Wandelt and T. Hoffmann, Hierarchical cosmic shear power spectrum inference, Monthly Notices of the Royal Astronomical Society **455** (2016) 4452 [1505.07840].

[49] J. Alsing, A. Heavens and A.H. Jaffe, Cosmological parameters, shear maps and power spectra from CFHTLenS using Bayesian hierarchical inference, Monthly Notices of the Royal Astronomical Society **466** (2017) 3272 [1607.00008].

[50] N. Porqueres, A. Heavens, D. Mortlock and G. Lavaux, Lifting weak lensing degeneracies with a field-based likelihood, Monthly Notices of the Royal Astronomical Society **509** (2022) 3194 [2108.04825].

[51] N. Jeffrey, F.B. Abdalla, O. Lahav, F. Lanusse, J.L. Starck, A. Leonard et al., Improving weak lensing mass map reconstructions using Gaussian and sparsity priors: application to DES SV, Monthly Notices of the Royal Astronomical Society **479** (2018) 2871 [1801.08945].

[52] A. Leonard, F. Lanusse and J.-L. Starck, GLIMPSE: accurate 3D weak lensing reconstructions using sparsity, Monthly Notices of the Royal Astronomical Society **440** (2014) 1281 [1308.1353].

[53] M.A. Price, J.D. McEwen, X. Cai, T.D. Kitching and LSST Dark Energy Science Collaboration, Sparse Bayesian mass mapping with uncertainties: peak statistics and feature locations, Monthly Notices of the Royal Astronomical Society **489** (2019) 3236 [1812.04018].

[54] P. Fiedorowicz, E. Rozo and S.S. Boruah, KaRMMa 2.0 – Kappa Reconstruction for Mass Mapping, arXiv e-prints (2022) arXiv:2210.12280 [2210.12280].

[55] P. Fiedorowicz, E. Rozo, S.S. Boruah, C. Chang and M. Gatti, KaRMMa - kappa reconstruction for mass mapping, Monthly Notices of the Royal Astronomical Society **512** (2022) 73 [2105.14699].

[56] J.L. Starck, S. Pires and A. Réfrégier, Weak lensing mass reconstruction using wavelets, Astronomy & Astrophysics **451** (2006) 1139 [astro-ph/0503373].

[57] J.L. Starck, K.E. Themelis, N. Jeffrey, A. Peel and F. Lanusse, Weak-lensing mass reconstruction using sparsity and a Gaussian random field, Astronomy & Astrophysics **649** (2021) A99 [2102.04127].

[58] Y. Shi, P. Zhang, Z. Sun and Y. Wang, Accurate kappa reconstruction algorithm for masked shear catalog, PHYSICAL REVIEW D **109** (2024) 123530.

[59] Y. Shi, P. Zhang, F. Deng, S. Zhou, H. Cai, J. Yao et al., Akra 2.0: Accurate kappa reconstruction algorithm for masked shear catalog, JOURNAL OF COSMOLOGY AND ASTROPARTICLE PHYSICS **2025** (2025) 038.

[60] R. Mandelbaum, H. Miyatake, T. Hamana, M. Oguri, M. Simet, R. Armstrong et al., The first-year shear catalog of the subaru hyper suprime-cam subaru strategic program survey, Publications of the Astronomical Society of Japan **70** (2018) .

[61] X. Liu, S. Yuan, C. Pan, T. Zhang, Q. Wang and Z. Fan, Cosmological studies from hsc-ssp tomographic weak-lensing peak abundances, Monthly Notices of the Royal Astronomical Society **519** (2023) 594.

[62] T. Lu, Z. Haiman and X. Li, Cosmological constraints from hsc survey first-year data using deep learning, Monthly Notices of the Royal Astronomical Society **521** (2023) 2050.

[63] L. Thiele, G.A. Marques, J. Liu and M. Shirasaki, Cosmological constraints from the subaru hyper suprime-cam year 1 shear catalogue lensing convergence probability distribution function, Physical Review D **108** (2023) .

[64] D. Grandón, G.A. Marques, L. Thiele, S. Cheng, M. Shirasaki and J. Liu, Impact of baryonic feedback on hsc-y1 weak lensing non-gaussian statistics, Physical Review D **110** (2024) .

[65] G.A. Marques, J. Liu, M. Shirasaki, L. Thiele, D. Grandón, K.M. Huffenberger et al., Cosmology from weak lensing peaks and minima with subaru hyper suprime-cam survey first-year data, Monthly Notices of the Royal Astronomical Society **528** (2024) 4513.

[66] C.P. Novaes, L. Thiele, J. Armijo, S. Cheng, J.A. Cowell, G.A. Marques et al., Cosmology from hsc y1 weak lensing with combined higher-order statistics and simulation-based inference, Cosmology from HSC Y1 Weak Lensing with Combined Higher-Order Statistics and Simulation-based Inference (2024) .

[67] J. Armijo, G.A. Marques, C.P. Novaes, L. Thiele, J.A. Cowell, D. Grandón et al., Cosmological constraints using minkowski functionals from the first year data of the hyper suprime-cam, Monthly Notices of the Royal Astronomical Society **537** (2025) 3553.

[68] S. Cheng, G.A. Marques, D. Grandón, L. Thiele, M. Shirasaki, B. Ménard et al., Cosmological constraints from weak lensing scattering transform using hsc y1 data, Journal of Cosmology and Astroparticle Physics **2025** (2025) .

[69] M. Tanaka, J. Coupon, B.C. Hsieh, S. Mineo, A.J. Nishizawa, J. Speagle et al., Photometric redshifts for hyper suprime-cam subaru strategic program data release 1, Publications of the Astronomical Society of Japan **70** (2018) .

[70] C. Hikage, M. Oguri, T. Hamana, S. More, R. Mandelbaum, M. Takada et al., Cosmology from cosmic shear power spectra with Subaru Hyper Suprime-Cam first-year data, Publications of the Astronomical Society of Japan **71** (2019) 43.

[71] T. Hamana, M. Shirasaki, S. Miyazaki, C. Hikage, M. Oguri, S. More et al., Cosmological constraints from cosmic shear two-point correlation functions with HSC survey first-year data, Publications of the Astronomical Society of Japan **72** (2020) .

[72] Z. Chen, Y. Yu, J. Han and Y. Jing, CSST cosmological emulator I: Matter power spectrum emulation with one percent accuracy to k = 10h Mpc^{-1}, Science China Physics, Mechanics, and Astronomy **68** (2025) 289512 [2502.11160].

[73] J. Han, M. Li, W. Jiang, Z. Chen, H. Wang, C. Wei et al., The Jiutian simulations for the CSST extra-galactic surveys, Science China Physics, Mechanics, and Astronomy **68** (2025) 109511 [2503.21368].

[74] Z. Chen and Y. Yu, CSST cosmological emulator II: Generalized accurate halo mass function emulation, Science China Physics, Mechanics, and Astronomy **68** (2025) 109513 [2506.09688].

[75] S. Zhou, Z. Chen and Y. Yu, CSST Cosmological Emulator III: Hybrid Lagrangian Bias Expansion Emulation of Galaxy Clustering, arXiv e-prints (2025) arXiv:2506.04671 [2506.04671].

[76] F. Bernardeau, L. van Waerbeke and Y. Mellier, Weak lensing statistics as a probe of OMEGA and power spectrum, Astronomy and Astrophysics **322** (1997) 1.

[77] A. Barthelemy, S. Codis and F. Bernardeau, Probability distribution function of the aperture mass field with large deviation theory, Monthly Notices of the Royal Astronomical Society **503** (2021) 5204.

[78] A. Boyle, C. Uhlemann, O. Friedrich, A. Barthelemy, S. Codis, F. Bernardeau et al., Nuw CDM cosmology from the weak lensing convergence PDF, Monthly Notices of the Royal Astronomical Society **505** (2021) 2886.

[79] A. Barthelemy, A. Halder, Z. Gong and C. Uhlemann, Making the leap. Part I. Modelling the reconstructed lensing convergence PDF from cosmic shear with survey masks and systematics, Journal of Cosmology and Astroparticle Physics **2024** (2024) 060.

[80] A. Taruya, M. Takada, T. Hamana, I. Kayo and T. Futamase, Lognormal Property of Weak-Lensing Fields, The Astrophysical Journal **571** (2002) 638.

[81] L. Clerkin, D. Kirk, M. Manera, O. Lahav, F. Abdalla, A. Amara et al., Testing the lognormality of the galaxy and weak lensing convergence distributions from Dark Energy Survey maps, Monthly Notices of the Royal Astronomical Society **466** (2017) 1444.

[82] S. van der Walt, S.C. Colbert and G. Varoquaux, The numpy array: A structure for efficient numerical computation, Computing in Science Engineering **13** (2011) 22.

[83] P. Virtanen, R. Gommers, T.E. Oliphant, M. Haberland, T. Reddy, D. Cournapeau et al., SciPy 1.0: Fundamental Algorithms for Scientific Computing in Python, Nature Methods **17** (2020) 261.

[84] K.M. Górski, E. Hivon, A.J. Banday, B.D. Wand elt, F.K. Hansen, M. Reinecke et al., HEALPix: A Framework for High-Resolution Discretization and Fast Analysis of Data Distributed on the Sphere, Astrophysical Journal **622** (2005) 759 [astro-ph/0409513].

[85] F. Perez and B.E. Granger, Ipython: A system for interactive scientific computing, Computing in Science Engineering **9** (2007) 21.

[86] N.E. Chisari, D. Alonso, E. Krause, C.D. Leonard, P. Bull, J. Neveu et al., Core Cosmology Library: Precision Cosmological Predictions for LSST, Astrophysical Journals **242** (2019) 2 [1812.05995].